

PARTICLE FORMATION IN OXYMETHYLENE ETHERS (OME_N , $N = 2-4$) / ETHYLENE PREMIXED FLAMES

ROBERT SCHMITZ¹, FEDERICA FERRARO^{1,*}, MARIANO SIRIGNANO², CHRISTIAN HASSE¹

¹ *Technical University of Darmstadt, Department of Mechanical Engineering, Simulation of reactive Thermo-Fluid Systems, Otto-Berndt-Str. 2, 64287 Darmstadt, Germany*

² *Dipartimento di Ingegneria Chimica, dei Materiali e della Produzione Industriale – Università degli Studi di Napoli Federico II, P. le Tecchio 80, 80125 Napoli, Italy*

ABSTRACT. Alternative synthetic fuels can be produced by renewable energy sources and represent a potential route for solving long-term energy storage. Among them, oxygenated fuels have the advantage of significantly reducing pollutant emissions and can therefore be used as carbon-neutral substitute fuels for transportation. In this work, the sooting propensity of different oxymethylene ethers (OME_n) is investigated using a combined experimental and numerical study on a series of burner-stabilized premixed flames under mild to severe sooting conditions. Herein, mixtures of ethylene in combination with the three individual OME_n for $n = 2-4$ are compared in terms of soot formation behavior with pure ethylene flames. The kinetic mechanism from Sun et al. (Proc. Combust. Inst. 36, 1269-1278, 2017) for oxymethylene ether OME_n combustion with $n=1-3$ is extended to include OME_4 decomposition and combustion kinetics. In the numerical simulations, the kinetic mechanism is combined with a detailed quadvariate soot model which uses the Conditional Quadrature Method of Moments and validated with Laser-Induced Fluorescence (LIF) and Laser-Induced Incandescence (LII) measurements. It is observed, that the three investigated OME_n with $n=2,3,4$ show similar sooting behavior, mainly reducing larger aggregates while not significantly affecting the formation of smaller particles. Furthermore, the extent of soot reduction is comparable among the three OME_n . The trends and overall reduction are very well captured by the model. The modeling results are analyzed through reaction path analyses and sensitivity studies which show the important role of OME_n decomposition and the formation of CH_2O under these rich conditions to reduce species relevant for soot formation. This is at the base of the negligible observed differences in terms of soot formation for the different OME_n fuels.

Keywords: Oxymethylene ethers (OMEn); Polyoxymethylene dimethyl ethers (PODEn); Soot formation; Alternative fuels; Quadrature Method of Moments (QMOM).

E-mail address: ferraro@stfs.tu-darmstadt.de.

1. INTRODUCTION

Oxygenated synthetic fuels can support the decarbonization of practical combustion devices reducing pollutant emissions especially in hard to electrify sectors such as maritime, heavy-duty and air transportation. Oxymethylene ethers (OMEs), $\text{CH}_3\text{O}(\text{CH}_2\text{O})_n\text{CH}_3$, also known as polyoxymethylene dimethyl ethers (PODEs or DMMs), are promising fuel candidates and are currently being investigated for self-ignition engine applications. They can be produced by renewable energy sources [1] yielding a neutral greenhouse gas balance. Recent studies have shown that OME fuels, pure or in blends, can significantly reduce carbon monoxide (CO), unburned hydrocarbons, and soot particles, e.g., [2–6]. Their molecular structure exhibits no C-C bonds, resulting in a fast oxidation process, a reduced amount of gas-phase particle precursors and particle formation.

Although combustion of pure OMEs yields an almost complete soot suppression [5], its application would require a redesign of available combustion systems. Therefore, the use of OMEs in blends with available fossil fuels is a practical pathway to reduce pollutant emission retrofitting available combustion systems. OMEs show good miscibility in fossil diesel [7, 8]. The cetane number of OME₂ to OME₅ [9, 10] as well as the flash, boiling and melting points are comparable to those of diesel fuel [8, 11], indicating their favorable use as fuel blends in compression ignition applications. Recently, reduced and detailed kinetic models have been developed for OME_n with $n = 1-3$ [7, 12–15], $n = 1-4$ [16], and $n = 1-6$ [17] and validated against experimental data for ignition delay time [12, 16, 18] and laminar flame speed [13]. OME blends have been studied under practical conditions in a high-pressure vessel [19] and in engine simulations [20, 21]. Investigations on soot formation for pure or blended OMEs in canonical flames have been conducted in [4–6]. The application of oxymethylene ethers in self-ignition engines in combination with their emission propensity has been studied in several works [21–28] showing that soot emissions are drastically reduced with OME_n in combination with conventional diesel fuel while breaking the tradeoff between soot and NO_x emission. In our recent work [4], 20 % of OME₃ blended with ethylene in premixed flames has been found to significantly affect the total number and the size of the particles produced. Specifically, the number of small particles with diameter $d_p < 5$ nm has been observed to remain unchanged or slightly increase, while the total amount of larger particles and aggregates with diameter $d_p > 20$ nm have been drastically reduced. Furthermore, soot structure has been investigated finding a slightly higher aromaticity for the pure ethylene soot. Particles produced from OME₃-doped flames contained larger amounts of oxygen, mainly in the form of C=O bonds.

Previous studies have been focused on OME₃ pure and in blends with traditional fuels (see e.g. [4, 5, 13, 21, 29]) due to its better low-temperature fluidity and volatility compared with OME₄ or larger compounds. OME_n with $n > 5$ exhibit a too high melting point, i.e., 18° C for OME₅ [8], while OME₁ is too volatile as a diesel additive [29]. However, OME production is achieved by multiple processes, which lead to a mix of OME_n at different level of polymerization [23, 30]. A commercially available OME mixture, with physico-chemical properties suitable for diesel applications, will therefore contain not only short-chain OME_n compounds, but also up to 30-wt% OME_{≥5} [8]. Hence, understanding the behaviour of the different OME_n compounds is of high practical relevance.

This work focuses on the comparative study of three OME_n fuels for $n = 2, 3$ and 4, combining experimental and numerical investigations to understand the features and potential differences in terms of particle emissions at different equivalence ratios, including lightly and highly sooting conditions.

Experimental investigations include quantitative measurements of particulate using in situ laser-based techniques, LIF and LII. A modification of the gas-phase kinetic mechanism employed in [4, 13], is then formulated to include OME₄ kinetics and validated with experimental data on particle formation.

Similar to [4, 5], the numerical investigations of the premixed sooting flames are conducted with the Conditional Quadrature Method of Moments (CQMOM) [31, 32], based on the physico-chemical soot model by D’Anna et al. [33]. In order to get more insights on the evolution of

OME fuels in flames, a detailed kinetic analysis to identify the main reaction pathways of OME_n oxidation up to the formation of gas-phase precursors has been conducted.

2. EXPERIMENTAL SETUP

Premixed flames burning ethylene as pure fuel and blended with 20 % of OME₂, OME₃ and OME₄ with equivalence ratios of $\phi = 2.01, 2.16, 2.31$ and 2.46 are stabilized on a capillary burner. OME_n, for $n = 2, 3$ or 4 , are added by replacing some of the ethylene (20 % of the total carbon fed), being ethylene/air flames the reference. Equivalence ratio, cold gas velocity and total carbon flow rate are kept constant while OME_n was added. In order to achieve this, nitrogen and oxygen streams are adapted accordingly. The same approach has been applied in previous works for other alternative fuels [4, 34] and references therein. The flame conditions investigated in this work are reported in Tab. 1.

TAB. 1. Flame inflow conditions given in mole fractions. OME_n indicates the mole fraction of OME₂, OME₃ and OME₄ in the corresponding flames, respectively.

ϕ		C ₂ H ₄ /O ₂ /N ₂	C ₂ H ₄ /OME ₂ /O ₂ /N ₂	C ₂ H ₄ /OME ₃ /O ₂ /N ₂	C ₂ H ₄ /OME ₄ /O ₂ /N ₂
2.01	OME _n	-	0.0123	0.0099	0.0082
	C ₂ H ₄	0.1234	0.0987	0.0987	0.0987
	N ₂	0.6925	0.7110	0.7147	0.7172
	O ₂	0.1841	0.1780	0.1767	0.1759
2.16	OME _n	-	0.0131	0.0105	0.0088
	C ₂ H ₄	0.1313	0.1051	0.1051	0.1051
	N ₂	0.6862	0.7055	0.7093	0.7119
	O ₂	0.1824	0.1763	0.1751	0.1743
2.31	OME _n	-	0.0139	0.0111	0.0093
	C ₂ H ₄	0.1392	0.1114	0.1114	0.1114
	N ₂	0.6800	0.7000	0.7040	0.7066
	O ₂	0.1808	0.1747	0.1735	0.1727
2.46	OME _n	-	0.0147	0.0118	0.0098
	C ₂ H ₄	0.1469	0.1175	0.1175	0.1175
	N ₂	0.6739	0.6946	0.6987	0.7015
	O ₂	0.1792	0.1732	0.1720	0.1712

Laser-Induced Emission (LIE) measurements in the 200–550 nm range are applied to detect particles in the flame, using the fourth harmonic of a Nd:YAG laser at 266 nm as the excitation source [4, 35]. The emitted spectra are collected with an ICCD camera with a gate of 100 ns, allowing to distinguish between the broad Laser-Induced Fluorescence (LIF) signal, ranging between 300 and 450 nm, and the Laser-Induced Incandescence (LII) following a blackbody curve and evaluated at 550 nm.

3. NUMERICAL MODELING

3.1. Gas-phase kinetics. In this work the kinetic mechanism employed in [4, 5], constituted by the detailed mechanism from D’Anna and co-workers [33] combined with the OME₁₋₃ kinetics from Sun et al. [13], is further developed. The kinetic mechanism is extended to cover the decomposition and combustion reactions of OME₄. Reaction pathways for OME₄ in analogy to smaller OMEs are added following the same reaction coefficients, similarly to the approach adopted by Sun et al. [13]. Similar to other OMEs, both formation of radicals and unimolecular decomposition are considered. Small fragments from OME₄ decomposition follow reaction pathways already established in previous mechanisms [4, 13]. In addition, according to considerations made in [4], a revised oxidation of CH₂O is proposed according to reaction rates found in the literature. The gas-phase kinetic mechanism extended for the OME₄ fuel consists in total of 757 reactions involving 154 species. It is worth noting that changes in CH₂O oxidation does not change the general

trend found for different OME_n compounds. Further details are discussed hereon. Temperature profiles measured in the experiments for the pure ethylene flames at different equivalence ratios are imposed in the simulations also for OME_n doped flames, similarly to the approach applied in [4]. Keeping constant equivalence ratio, cold gas velocity and total carbon flow rate when OME_n are added allow to have a negligible impact on the temperature profile, as verified for other oxygenated fuels [35].

3.2. Soot modeling. A detailed physico-chemical soot formation model [33] combined with the Conditional Quadrature Method of Moments (CQMOM) is employed to study the sooting properties of OME_2 to OME_4 . The numerical approach developed in [31] has been successfully applied in atmospheric premixed flames in [4, 31, 32]. The gas phase kinetics account for species up to pyrene, while PAH compounds with a molecular weight larger than pyrene are not treated as individual species but considered as lumped species (*large PAHs*), whose evolution is described by the CQMOM. The soot model distinguishes between three different particle structures based on their state of aggregation [33]: *large PAHs*, *clusters* and *aggregates*. *Clusters* are spherically shaped, solid soot particles formed by the inception steps involving *large PAHs*. *Aggregates* are fractal-shaped particles generated by the aggregation of several *clusters*.

The evolution of the chemical and physical properties of each particle class is described by the population balance equation (PBE) for the number density function (NDF) $f(\underline{\xi}; \underline{x}, t)$, which depends on the spatial coordinates \underline{x} , the time t and the internal property vector $\underline{\xi}$ with

$$\underline{\xi} = [\xi_{nc}, \xi_{H/C}, \xi_{stat}, \xi_{typ}]^T. \quad (1)$$

$\underline{\xi}$ contains two continuous properties ξ_{nc} , indicating the number of carbon atoms with $\xi_{nc} \in [0, \infty)$, and $\xi_{H/C}$ describing the carbon to hydrogen ratio with $\xi_{H/C} \in [0, 1]$. ξ_{typ} and ξ_{stat} are discrete dimensions representing the type of entities $\xi_{typ} \in A$, $A = \{\textit{large PAHs}, \textit{clusters}, \textit{aggregates}\}$, and ξ_{stat} the chemical reactivity with $\xi_{stat} \in B$, $B = \{\textit{stable}, \textit{radical}\}$.

The CQMOM is used to solve the quadrivariate NDF. Following [31] the quadrivariate NDF is reformulated in six bivariate NDFs and a set of 36 statistical moments are solved to account for the soot particle evolution. Further details on the numerical approach can be found in [31, 32].

The soot processes, which provide the moment source terms, are formulated based on Arrhenius-rate laws and include growth processes such as the H-Abstraction- C_2H_2 -Addition (HACA) mechanism, the resonantly stabilized free radical mechanism or surface growth due to chemical processes. Nucleation steps for different-sized large PAHs are accounted for, resulting in clusters with various chemical properties as well as oxidation and oxidation-induced fragmentation, dehydrogenation and aggregation processes of several clusters, resulting chain-like formed aggregates.

4. RESULTS

Firstly, experimental and numerical results for gas-phase species and soot formation in ethylene and ethylene/ OME_n flames are presented. Then, reaction pathways flux analyses are performed for the richest condition $\phi = 2.46$ to characterize the decomposition of the investigated OME_n . Additionally, the influence of selected OME_n reactions on formaldehyde formation is evaluated with a sensitivity study.

4.1. Gas-phase analysis and soot formation in OME_2 , OME_3 , and OME_4 blended flames. Modeled mole fraction profiles for selected species in the investigated flames with pure ethylene fuel and OME_n /ethylene blended mixtures are here analyzed. Other major species such as CO, H and H_2 , not shown here for brevity, are almost insensitive to the OME_n blending, while a slightly higher amount of CO_2 is formed with the addition of OME_n compounds as expected. Generally, a better oxidation mechanism for OME_n is expected due to the absence of C-C bonds in the fuel structure. Methane (CH_4) and formaldehyde (CH_2O), which are key species during the decomposition process of OME_n as well as acetylene (C_2H_2) and benzene (C_6H_6), which are important soot precursor species, are plotted in Fig. 1 for the four equivalence ratios and fuel

mixtures against the height above the burner (HAB). As expected, CH_4 and CH_2O increase in the OME_n doped flames compared to the pure ethylene flames. In particular, CH_4 is significantly higher in concentration in OME_n doped flames as equivalence ratios increase, suggesting a more effective decomposition process. A clear peak in the profiles is visible for CH_2O close to the inlet, again because of fast oxidation/decomposition pathways, then CH_2O quickly decomposes further downstream to smaller species. In general, the preferential pathways leading to the formation of CH_2O suggest a fast decomposition and a more complete combustion process when OME_n are used in comparison to the pure ethylene.

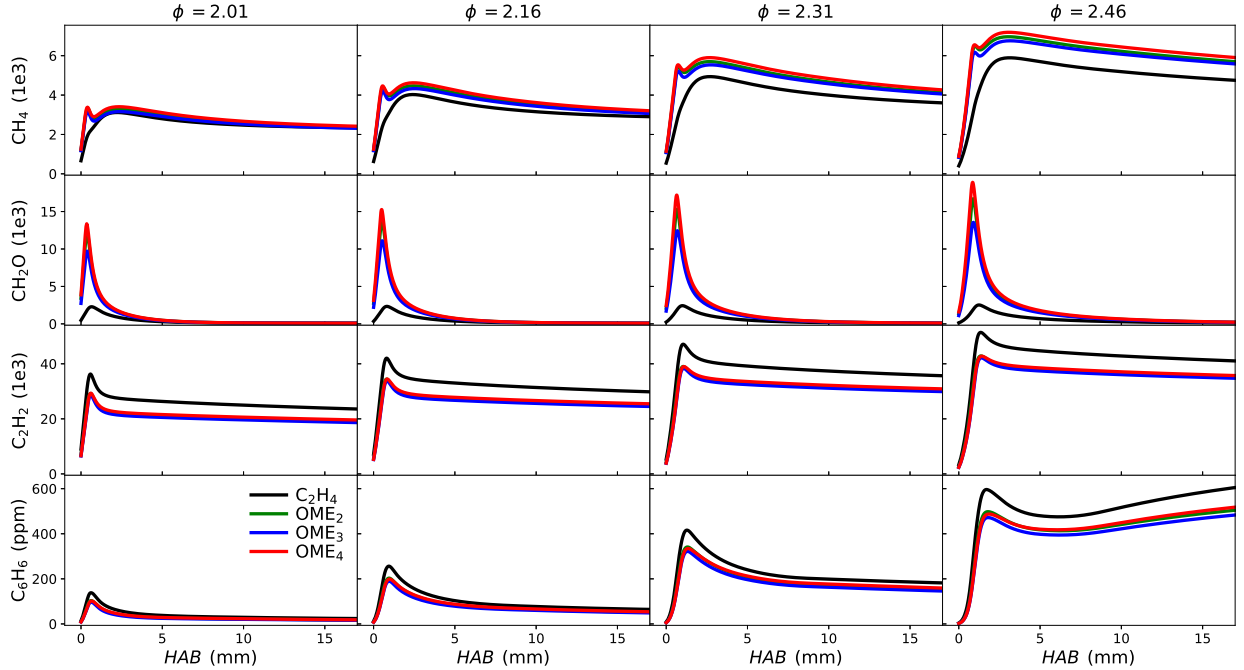


FIG. 1. Species mole fraction profiles of CH_4 , CH_2O , C_2H_2 and C_6H_6 as a function of height above the burner HAB obtained for pure ethylene and OME_n /ethylene blended mixtures for $n = 2, 3, 4$ at different equivalence ratios.

OME doping inhibits the formation of species relevant for particle formation and growth such as C_2H_2 and C_6H_6 . These species lead to the formation of intermediate soot precursors and directly contribute in the soot formation process due to surface growth by HACA process or deposition onto the particle surface (by C_6H_6 or larger PAHs). C_2H_2 is constantly higher in pure ethylene flames across all the equivalence ratios because it is mostly coming from ethylene dehydrogenation pathways. Hence, C_2H_2 mainly depends on the amount of ethylene present in the blend disregarding of the equivalence ratio investigated. The effect of OME_n is indeed of the first order on this species and a larger effect on particle formation is expected at higher equivalence ratios where surface growth plays a major role. On the other side, the reduction of C_6H_6 increases as equivalence ratio increases, due to relation of C_6H_6 formation to intermediate C3 and C4 compounds. The effect of C_6H_6 on particle is more complex to follow since it has a direct effect on PAH formation, hence slowing down inception process. This is likely to have a significant effect also at lower equivalence ratio where the inception mechanism is the controlling process for particle formation. Overall it is interesting to see that both the profile shape and the mole fraction values for all the key species plotted and for all the equivalence ratios show negligible differences for the different OME_n . This suggests similar soot formation behavior of the different OME_n compounds.

Figure 2 shows the modeling results for particles compared with experimentally measured nanoparticles and soot particles for the investigated equivalence ratios and different OME_n -blended mixtures. As done in previous works, here LIF signal is associated with aromatic hydrocarbons in condensed-phase, i.e. nanoparticles [36], whereas the LII signal is referred to solid soot particles

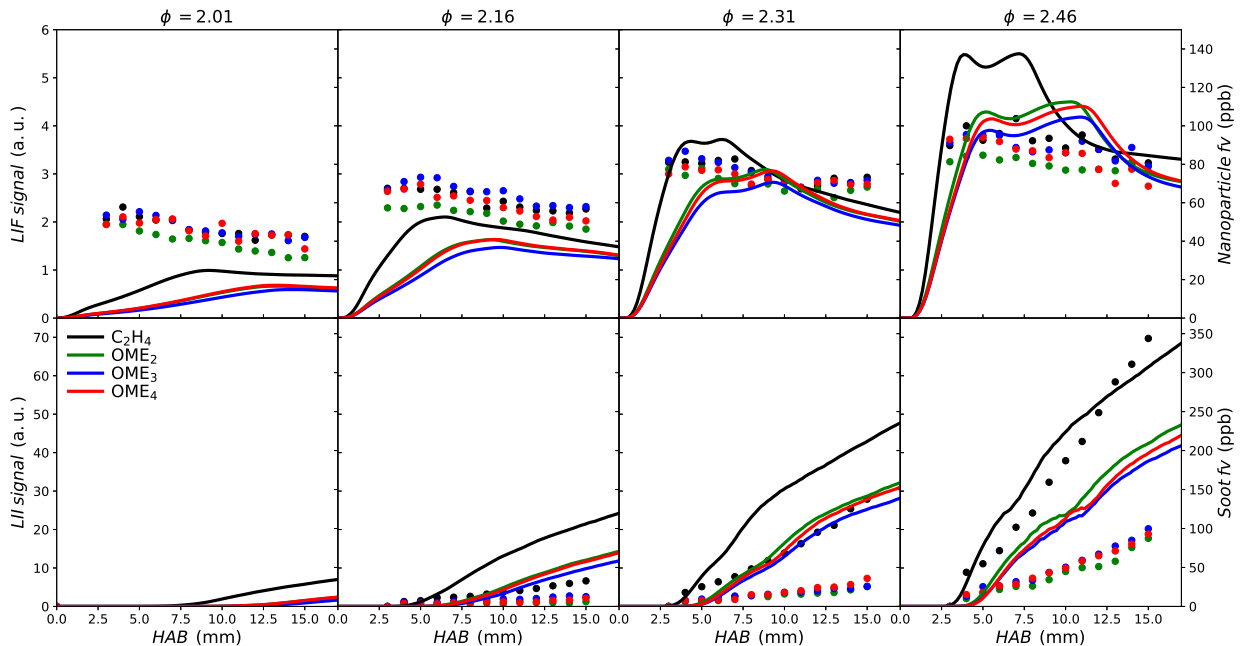


FIG. 2. Comparison of the simulated nanoparticle volume fraction against the measured LIF signal (top row) and the simulated soot volume fraction against the measured LII signal (bottom row) for the four investigated equivalence ratios and fuel compositions. Lines indicate predicted profiles simulated using the quadrivariate CQMOM model whereas dots represent experimental data. The pure ethylene flame is colored black and the OME_n doped flames are colored green, blue and red representing OME_2 , OME_3 and OME_4 fuel addition to the flame.

and aggregates. In order to better compare modeling results with experimental data, following previous studies [4, 32], the total amount of particles modelled is split depending on particle diameter. Specifically, nanoparticle volume fraction includes particles smaller than the split diameter $d_{p,split}$, while soot volume fraction includes particles with a diameter larger than $d_{p,split}$. Splitting process is here performed varying the value of split particle diameter, i.e., for $d_{p,split} = 2$ nm and $d_{p,split} = 7$ nm, to reduce the sensitivity of the results on the selected value. The plotted volume fraction fv is obtained as the average of both splitting processes. The error bars are not reported here for the sake of clarity, however as shown in previous works the choice of $d_{p,split}$ is not affecting the profile shape nor the absolute value of the nanoparticles volume fraction.

In previous studies [4, 5] it has been found that OME_3 addition reduces the formation of large soot aggregates significantly, while the formation of smaller nanoparticles is less affected. The LIF measurements in Fig. 2 suggest similar trends for OME_2 and OME_4 doped flames. There is indeed no noticeable difference of the LIF signal for the pure C_2H_4 flame compared to OME_3 and OME_4 doped flames, the OME_2 doped flame exhibits the smallest signal value while still being close to the other results and within the measurement uncertainty. The simulation results of the nanoparticle formation show minor differences for OME_n compounds and therefore reproducing the trends observed in the experiments. The model reproduces a slowing down of the particle formation process. Despite the model slightly overpredicting the nanoparticle peak in the richest ethylene flame, it can reproduce the trend of nanoparticle concentration for ethylene and OME_n blends. Overall it is interesting to note that all the OMEs behave similarly to other oxygenated fuels [35], having a minor impact of the total formation of small nanoparticles, which dominate particle size distribution in terms of number [4].

LII measurements show the onset of soot formation at an equivalence ratio of $\phi = 2.16$ for all OME_n mixtures, while no soot is measured for $\phi = 2.01$. Furthermore, soot reduction for the three investigated OME_n compounds at higher equivalence ratios is comparable. Thus, the experimental

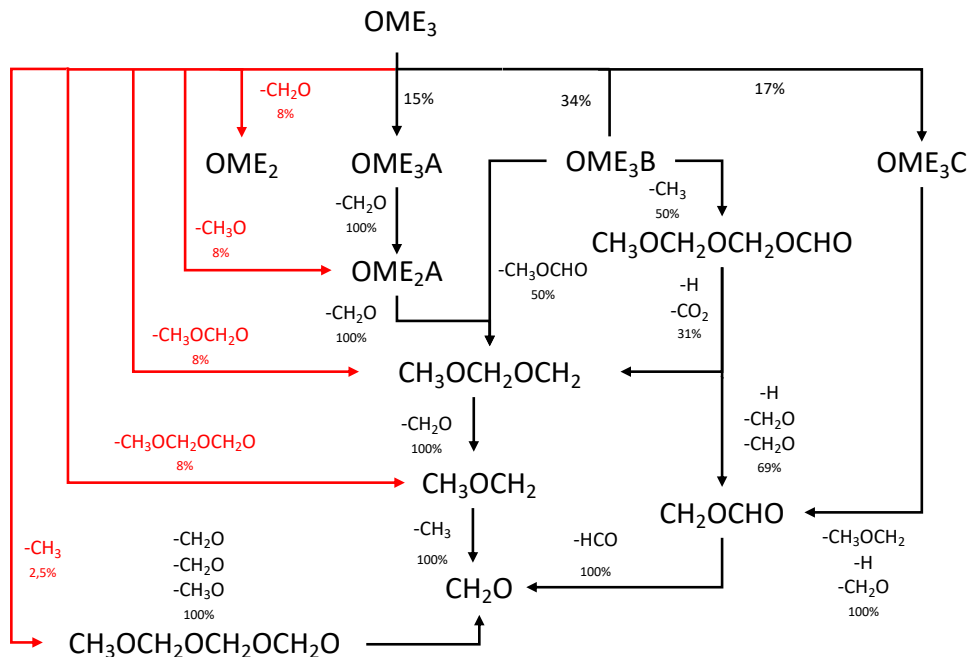


FIG. 3. Reaction pathways for OME_3 based on the integrated carbon flux for the $\text{C}_2\text{H}_4/\text{OME}_3/\text{O}_2/\text{N}_2$ mixture at $\phi = 2.46$. The numbers are the flux percent contribution relative to the species on the source side. The red lines indicate the unimolecular decomposition pathways. According to [13], DMM3A: $\text{CH}_3\text{OCH}_2\text{OCH}_2\text{OCH}_2\text{OCH}_2$; DMM3B: $\text{CH}_3\text{OCH}_2\text{OCH}_2\text{OCHOCH}_3$; DMM3C: $\text{CH}_3\text{OCH}_2\text{OCHOCH}_2\text{OCH}_3$; DMM2A: $\text{CH}_3\text{OCH}_2\text{OCH}_2\text{OCH}_2$.

results indicate that the reduction of large aggregates is similar for mixtures blended with OME_2 , OME_3 and OME_4 .

Regarding the simulation results, the significant reduction of large particles due to OME_2 , OME_3 and OME_4 addition is well captured by the model. Nevertheless, the overall soot reduction predicted by the model is less than the one observed in the experiments. Compared to the previous results for OME_3 mixtures [4], the formaldehyde decomposition of the base mechanism has been revised resulting in a larger soot reduction up to 40 % in terms of large particles in the richest condition for the OME_3 and OME_4 flames, which is closer to the measurement results of around 70 %, yielding a significant improvement compared to the kinetic mechanism used in [4], where soot reduction of approx. 25 % was numerically achieved. Furthermore, these results confirm the validity of the approach applied to extend the gas-phase kinetics originally developed by Sun et al. [13] for $n = 1-3$ to $n = 1-4$ for the investigated conditions.

4.2. Reaction analysis. The gas-phase kinetics is further analyzed to identify the main reaction pathways under rich flame conditions and better understand the reaction pathways for different OME_n . Figure 3 schematically displays the reaction pathways of the OME_3 decomposition to smaller species for a $\text{C}_2\text{H}_4/\text{OME}_3/\text{O}_2/\text{N}_2$ mixture at an equivalence ratio of $\phi = 2.46$ and temperature $T = 1500$ K. The composition of the gas phase is according to Tab. 1. The carbon flux indicates that for OME_3 oxidation/decomposition pathways lead rapidly to CH_2O formation. The importance of this latter in OME_n rich combustion is hence crucial and its oxidation/decomposition determines the overall particle reduction. Furthermore, it is observed that in the conditions analyzed in this study the unimolecular pathways, almost irrelevant (<1 %) in the conditions analyzed by Sun et al. (cfr. Fig. 5 in [13]), are here significant. Almost 34 % of the carbon contained in the OME_3 fuel is indeed decomposed through unimolecular decomposition reactions. Similar trends

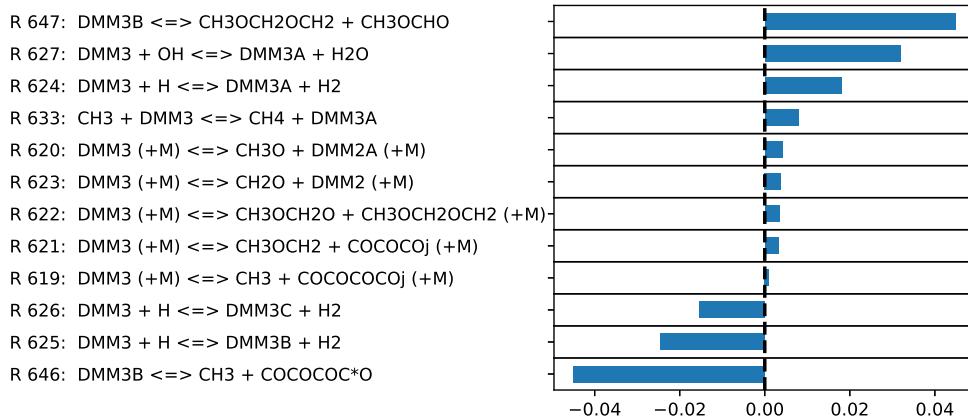


FIG. 4. Sensitivity of the CH_2O mole fraction peak for small perturbations of different reaction rates in the richest OME_3 flame. According to [13], DMM3: $\text{CH}_3\text{OCH}_2\text{OCH}_2\text{OCH}_2\text{OCH}_3$; DMM3A: $\text{CH}_3\text{OCH}_2\text{OCH}_2\text{OCH}_2\text{OCH}_2$; DMM3B: $\text{CH}_3\text{OCH}_2\text{OCH}_2\text{OCHOCH}_3$; DMM3C: $\text{CH}_3\text{OCH}_2\text{OCHOCH}_2\text{OCH}_3$; DMM2: $\text{CH}_3\text{OCH}_2\text{OCH}_2\text{OCH}_3$; DMM2A: $\text{CH}_3\text{OCH}_2\text{OCH}_2\text{OCH}_2$; COCOCOCoj: $\text{CH}_3\text{OCH}_2\text{OCH}_2\text{OCH}_2\text{O}$; COCOCOCoj: $\text{CH}_3\text{OCH}_2\text{OCH}_2\text{O}$; COCOCOC*O: $\text{CH}_3\text{OCH}_2\text{OCH}_2\text{OCHO}$.

have been observed in the reaction pathway analysis for OME_2 ($\approx 40\%$) and OME_4 ($\approx 38\%$) which are not shown here for brevity. Large amounts of CH_2O and other aldehydic compounds are formed during OME_n combustion, whereas almost no other oxygenated species are produced. This could be linked with the presence of a specific oxygen functionality onto particles found experimentally [4]. Further investigation on this point is needed.

Finally, Fig. 4 shows the sensitivity of the CH_2O mole fraction peak in the OME_3 flame with an equivalence ratio of $\phi = 2.46$ for a small change ($k = 0.5\%$) of the reaction rate coefficients of selected reactions decomposing OME_3 into radicals and smaller species. Sensitivity analysis confirms the general picture seen in reaction pathway analysis for CH_2O formation. Formation of DMM3A radical and the breaking of OME_3 into small fragments strongly favor CH_2O formation. On the other side, DMM3B radical and even more DMM3C radical have a negative impact on CH_2O formation, slowing down the process. DMM3B eventually decomposing towards small fragments (R647) would recover its capability of fast producing CH_2O . Similar results are obtained for OME_2 and OME_4 . Sensitivity analysis for OME_2 shows a strong preference of DMM2A radical for CH_2O formation without possibility of recovering for DMM2B. On the other side for OME_4 , the only radical that inhibits CH_2O formation is DMM4C, being DMM4B fast breaking into small fragments and favor CH_2O formation.

5. CONCLUSIONS

The sooting propensity of different OME_n compounds for $n = 2, 3, 4$ was investigated by combining experimental measurements with numerical simulations. Ethylene flames with equivalence ratios $\phi = 2.01, 2.16, 2.31, 2.46$ blended with 20 % of different OME_n compounds were studied. Experimental LIF and LII measurements for these flames were performed which exhibited similar trends for the soot formation properties of the three OME_n investigated. The addition of all OME_n compounds primarily reduces the formation of larger soot particles compared to pure ethylene flames, while the formation of smaller particles is less affected. A comparable total amount of soot particle reduction for the three OME_n was observed. Furthermore, the kinetic mechanism from Sun et al. [13] for OME_{1-3} was extended with OME_4 kinetics. Numerical simulations were performed using the detailed mechanism kinetic mechanism in combination with the CQMOM soot model. The experimentally observed trends of the soot reduction are very well reproduced

by the model for all OME_n compounds. Reaction pathway analyses and sensitivity studies for the OME_n show the importance of the fuel decomposition under the investigated conditions for CH₂O formation. Overall, within the investigated conditions, different OME_n have shown similar kinetic behavior, suggesting that some differences could arise if the first steps of oxidation/decomposition might become slow enough to be the controlling steps.

ACKNOWLEDGMENTS

The authors gratefully acknowledge the funding by the German Federal Ministry of Education and Research (BMBF) as part of the NAMOSYN Project (project number 03SF0566R0).

REFERENCES

- [1] Yann Fenard and Guillaume Vanhove. A Mini-Review on the Advances in the Kinetic Understanding of the Combustion of Linear and Cyclic Oxymethylene Ethers. *Energy and Fuels*, 35(18):14325–14342, 2021.
- [2] Zhi Wang, Haoye Liu, Xiao Ma, Jianxin Wang, Shijin Shuai, and Rolf D. Reitz. Homogeneous charge compression ignition (HCCI) combustion of polyoxymethylene dimethyl ethers (PODE). *Fuel*, 183:206–213, 2016.
- [3] Haoye Liu, Zhi Wang, Jianxin Wang, and Xin He. Improvement of emission characteristics and thermal efficiency in diesel engines by fueling gasoline/diesel/PODEn blends. *Energy*, 97:105–112, 2016.
- [4] Federica Ferraro, Carmela Russo, Robert Schmitz, Christian Hasse, and Mariano Sirignano. Experimental and numerical study on the effect of oxymethylene ether-3 (OME3) on soot particle formation. *Fuel*, 286:119353, feb 2021.
- [5] Robert Schmitz, Mariano Sirignano, Christian Hasse, and Federica Ferraro. Numerical Investigation on the Effect of the Oxymethylene Ether-3 (OME3) Blending Ratio in Premixed Sooting Ethylene Flames. *Front. Mech. Eng.*, 7:1–11, 2021.
- [6] Yong Ren Tan, Maurin Salamanca, Laura Pascazio, Jethro Akroyd, and Markus Kraft. The effect of poly(oxymethylene) dimethyl ethers (PODE3) on soot formation in ethylene/PODE3 laminar coflow diffusion flames. *Fuel*, 283:118769, 2021.
- [7] Qinjie Lin, Kun Lin Tay, Dezhi Zhou, and Wenming Yang. Development of a compact and robust Polyoxymethylene Dimethyl Ether 3 reaction mechanism for internal combustion engines. *Energy Convers. Manag.*, 185:35–43, 2019.
- [8] Ahmad Omari, Benedikt Heuser, Stefan Pischinger, and Christoph Rüdinger. Potential of long-chain oxymethylene ether and oxymethylene ether-diesel blends for ultra-low emission engines. *Appl. Energy*, 239:1242–1249, 2019.
- [9] Ludger Lautenschütz, Dorian Oestreich, Philipp Seidenspinner, Ulrich Arnold, Eckhard Dinjus, and Jörg Sauer. Physico-chemical properties and fuel characteristics of oxymethylene dialkyl ethers. *Fuel*, 173:129–137, 2016.
- [10] Diana Deutsch, Dorian Oestreich, Ludger Lautenschütz, Philipp Haltenort, Ulrich Arnold, and Jörg Sauer. High Purity Oligomeric Oxymethylene Ethers as Diesel Fuels. *Chemie-Ingenieur-Technik*, 89:486–489, 2017.
- [11] Y. Zheng, Q. Tang, T. Wang, Y. Liao, and J. Wang. Synthesis of a green fuel additive over cation resins. *Chem. Eng. Technol.*, 36(11):1951–1956, 2013.
- [12] Tanjin He, Zhi Wang, Xiaoqing You, Haoye Liu, Yingdi Wang, Xiaoyu Li, and Xin He. A chemical kinetic mechanism for the low- and intermediate-temperature combustion of Polyoxymethylene Dimethyl Ether 3 (PODE3). *Fuel*, 212:223–235, 2018.
- [13] Wenyu Sun, Guoqing Wang, Shuang Li, Ruzheng Zhang, Bin Yang, Jiuzhong Yang, Yuyang Li, Charles K. Westbrook, and Chung K. Law. Speciation and the laminar burning velocities of poly(oxymethylene) dimethyl ether 3 (POMDME3) flames: An experimental and modeling study. *Proc. Combust. Inst.*, 36(1):1269–1278, 2017.
- [14] Runzhao Li, Jose Martin Herreros, Athanasios Tsolakis, and Wenzhao Yang. Chemical kinetic study on ignition and flame characteristic of polyoxymethylene dimethyl ether 3 (PODE3). *Fuel*, 279:118423, 2020.

- [15] Yuwei Zhao, Ning Li, Yijing Xie, Yuemeng Cheng, and Xiaochen Wang. Study on chemical kinetic mechanisms of Polyoxymethylene Dimethyl Ethers (PODE_n). *IOP Conf. Ser. Mater. Sci. Eng.*, 768(2):022056, mar 2020.
- [16] Liming Cai, Sascha Jacobs, Raymond Langer, Florian vom Lehn, Karl Alexander Heufer, and Heinz Pitsch. Auto-ignition of oxymethylene ethers (OMEn, n = 2–4) as promising synthetic e-fuels from renewable electricity: shock tube experiments and automatic mechanism generation. *Fuel*, 264:116711, 2019.
- [17] Bo Niu, Ming Jia, Yachao Chang, Huiquan Duan, Xue Dong, and Pengzhi Wang. Construction of reduced oxidation mechanisms of polyoxymethylene dimethyl ethers (PODE1–6) with consistent structure using decoupling methodology and reaction rate rule. *Combust. Flame*, 232:111534, 2021.
- [18] Kevin De Ras, Marvin Kusenbergh, Guillaume Vanhove, Yann Fenard, Andreas Eschenbacher, Robin J. Varghese, Jeroen Aerssens, Ruben Van de Vijver, Luc-Sy Tran, Joris W. Thybaut, and Kevin M. Van Geem. A detailed experimental and kinetic modeling study on pyrolysis and oxidation of oxymethylene ether-2 (OME-2). *Combust. Flame*, 238:111914, 2022.
- [19] Dominik Goeb, Marco Davidovic, Liming Cai, Pankaj Pancharia, Mathis Bode, Sascha Jacobs, Joachim Beeckmann, Werner Willems, Karl Alexander Heufer, and Heinz Pitsch. Oxymethylene ether – n-dodecane blend spray combustion: Experimental study and large-eddy simulations. *Proc. Combust. Inst.*, 38(2):3417–3425, 2021.
- [20] Delin Lv, Yingjie Chen, Yaojuan Chen, Xiaoyu Guo, Hui Chen, and Haozhong Huang. Development of a reduced diesel/PODE_n mechanism for diesel engine application. *Energy Convers. Manag.*, 199:112070, 2019.
- [21] Shuojin Ren, Zhi Wang, Bowen Li, Haoye Liu, and Jianxin Wang. Development of a reduced polyoxymethylene dimethyl ethers (PODE_n) mechanism for engine applications. *Fuel*, 238:208–224, 2019.
- [22] Matteo Parravicini, Christophe Barro, and Konstantinos Boulouchos. Compensation for the differences in LHV of diesel-OME blends by using injector nozzles with different number of holes: Emissions and combustion. *Fuel*, 259:116166, 2020.
- [23] Dominik Pélerin, Kai Gaukel, Martin Härtl, Eberhard Jacob, and Georg Wachtmeister. Potentials to simplify the engine system using the alternative diesel fuels oxymethylene ether OME1 and OME3-6 on a heavy-duty engine. *Fuel*, 259:116231, 2020.
- [24] Leonardo Pellegrini, Mario Marchionna, Renata Patrini, and Salvatore Florio. Emission performance of neat and blended polyoxymethylene dimethyl ethers in an old light-duty diesel car. *SAE Tech. Pap.*, 2, 2013.
- [25] Christophe Barro, Matteo Parravicini, Konstantinos Boulouchos, and Anthi Liati. Neat polyoxymethylene dimethyl ether in a diesel engine; part 2: Exhaust emission analysis. *Fuel*, 234:1414–1421, 2018.
- [26] Haozhong Huang, Qingsheng Liu, Wenwen Teng, Mingzhang Pan, Chang Liu, and Qingxin Wang. Improvement of combustion performance and emissions in diesel engines by fueling n-butanol/diesel/PODE3–4 mixtures. *Appl. Energy*, 227:38–48, 2018.
- [27] Simon LeBlanc, Navjot Sandhu, Xiao Yu, Xiaoye Han, Meiping Wang, Jimi Tjong, and Ming Zheng. An Investigation Into OME3 on a High Compression Ratio Engine. In *ASME 2020 Intern. Combust. Engine Div. Fall Tech. Conf.*, 2020. ISBN 978-0-7918-8403-4.
- [28] Haoye Liu, Zhi Wang, Yanfei Li, Yanyan Zheng, Tanjin He, and Jianxin Wang. Recent progress in the application in compression ignition engines and the synthesis technologies of polyoxymethylene dimethyl ethers. *Appl. Energy*, 233-234:599–611, 2019.
- [29] B. Lumpp, D. Rothe, C. Pastotter, R. Lämmermann, and Eberhard Jacob. Oxymethylene Ethers As Diesel Fuel. *Mtz Worldw.*, 78:34–38, 2011.
- [30] Oluchi Emenike, Stavros Michailos, Kevin J. Hughes, Derek Ingham, and Mohamed Pourkashanian. Techno-economic and environmental assessment of BECCS in fuel generation for FT-fuel, bioSNG and OME_x. *Sustain. Energy Fuels*, 5:3382–3402, 2021.
- [31] Steffen Salenbauch, Mariano Sirignano, Daniele L. Marchisio, Martin Pollack, Andrea D’Anna, and Christian Hasse. Detailed particle nucleation modeling in a sooting ethylene flame using

- a Conditional Quadrature Method of Moments (CQMOM). *Proc. Combust. Inst.*, 36:771–779, 2017.
- [32] Steffen Salenbauch, Mariano Sirignano, Martin Pollack, Andrea D’Anna, and Christian Hasse. Detailed modeling of soot particle formation and comparison to optical diagnostics and size distribution measurements in premixed flames using a method of moments. *Fuel*, 222:287–293, jun 2018.
- [33] Andrea D’Anna, Mariano Sirignano, and John Kent. A model of particle nucleation in premixed ethylene flames. *Combust. Flame*, 157:2106–2115, 2010.
- [34] Marielena Conturso, Mariano Sirignano, and Andrea D’Anna. Effect of 2,5-dimethylfuran doping on particle size distributions measured in premixed ethylene/air flames. *Proc. Combust. Inst.*, 36:985–992, 2017.
- [35] Marielena Conturso, Mariano Sirignano, and Andrea D’Anna. Effect of furanic biofuels on particles formation in premixed ethylene-air flames: An experimental study. *Fuel*, 175:137–145, 2016.
- [36] Mariano Sirignano, Daniel Bartos, Marielena Conturso, Matthew Dunn, Andrea D’Anna, and Assaad R. Masri. Detection of nanostructures and soot in laminar premixed flames. *Combust. Flame*, 176:299–308, 2017.